Proceedings of the
Annual Stability Conference
Structural Stability Research Council
Louisville, Kentucky April 14-16, 2021

Classical and finite element methods for elastic buckling of cylindrical shells

V. Ding[1], A.H.A. Abdelrahman[2], D. Lin[3],
M.D. Shields[4], A.T. Myers[5], M. Krabbe[6], B.W. Schafer[7]

Abstract

The objective of this paper is to provide and evaluate classical and finite element method solutions for the elastic buckling of thin cylindrical shells appropriate for applications in steel wind turbine towers. Particular attention is given to two features of wind turbine towers: (1) the diameter-to-thickness ratio can be quite high with ratios regularly in the range of 110 and already today having maximum diameter-to-thickness ratios exceeding 250, and (2) the towers are subject to relatively complex loading including compression, bending, shear, and torsion. A set of specific tube geometries, consistent with planned future testing, are presented and examined. Critical buckling stresses and buckling modes are studied using both classical analytical methods and shell finite element methods. Particular attention is paid to understanding the role of circumferential and longitudinal buckling half-wavelengths in the classical solutions across the considered loading cases and how these same solutions are realized in the shell finite element models. While it is well known that the elastic buckling solution is a poor predictor of ultimate strength, elastic buckling still plays a strong role in our understanding of the imperfection sensitivity of these structures – particularly under complex combined loading cases that have not seen significant study to date. This paper provides the initial basis for forthcoming experiments and future nonlinear collapse simulations with random field imperfection models that are primary goals in future studies.

[1] Ph.D. Candidate, Johns Hopkins University, USA <vding1@jhu.edu>
[2] Lecturer, Mansoura University, Egypt <a_hussain@mans.edu.eg>
[3] Ph.D. Candidate, Northeastern University, USA <lin.deh@northeastern.edu>
[4] Associate Professor, Johns Hopkins University, USA <michael.shields@jhu.edu>
[5] Associate Professor, Northeastern University, USA <an.myers@northeastern.edu>
[6] Assistant Lead Engineer, Vestas, DK <madsk@vestas.com>
[7] Professor, Johns Hopkins University, USA <schafer@jhu.edu>

1. Introduction

The stability of thin shells is a longstanding problem in structural stability. Standards of practice for a variety of structural engineering applications that utilize thin shells have been successfully established and utilized by engineers, see e.g. ECCS (2007), Rotter and Schmidt (2013). However, each time engineers desire to move into new domains for thin shells they are once again faced with the extreme imperfection sensitivity in the structural response of these members and forced to develop adequate procedures for their design.

Today, one such application for thin shells of interest is the use of thin steel cylindrical tubes as supporting towers for wind turbines to produce renewable energy. Creating structurally efficient/optimized towers is one means by which tower heights can be increased thereby providing the turbines with higher and more consistent winds (Jay et al. 2016). In addition, the materials required for the tower design increase the carbon footprint of the tower itself, so sustainability goals for the structure also push towards the most efficient possible use of the material. Of course nothing is more wasteful than a structural tower failure, therefore structural efficiency must be balanced by structural reliability. Further complicating the problem are some of the specifics of wind turbine tower design: the balance between fatigue and stability driven failures, the relatively complex loading actions that can create unique bending and torsion demands on the same segment of tower, and additional considerations (DNV 2002).

In this paper we start at the beginning – elastic buckling. Though it is well known that elastic buckling is not directly useful in design it still is a useful parameter for characterizing tower slenderness and part of almost any analytical design method (e.g. ECCS 2007, Rotter 2016). Further, elastic buckling has long been tied to our understanding of imperfection sensitivity in these thin shells (Koiter, 1945), so a full understanding of the relevant elastic buckling problems is beneficial for understanding the key factors in their response sensitivity. In particular, in this paper we focus on elastic buckling in compression, bending, and torsion for long cylindrical tubes with diameter-to-thickness ratios (D_c/t) between 100 and 350. This paper begins with an examination of current and future parameter ranges for steel monopole wind turbine towers, then provides a summary of the elastic buckling response using analytical expressions followed by shell finite element models. Particular attention is given to a range of scaled geometries that are consistent with future laboratory testing. The paper concludes with a discussion of the implications of the elastic buckling results and an introduction to future work planned by the research team.

2. Steel Monopole Wind Turbine Towers

For a thorough discussion of the design of steel monopole wind turbine towers see DNV (2002). Here we focus only on the static stability behavior and ignore fatigue limit states and the large variety of details required to produce a serviceable tower. Instead here we limit discussion to three major issues (1) the overall slenderness of typical towers, (2) the critical loading actions on the towers, and (3) the introduction of several scaled geometries that are being considered for laboratory scale testing.

2.1 Slenderness (D_c/t)

Wind turbine towers are not shaped as perfect cylindrical tubes. Fig. 1 provides a scaled drawing of a typical steel monopole wind turbine tower. Short cylindrical cans, shown between dashed lines in Fig. 1, are fabricated and then welded together to form longer segments, shown between solid lines in Fig. 1. Segments are connected by ring stiffeners. The D_c/t is unique to each can, but along the tower height the D_c varies to provide an overall taper and the t varies to accommodate the actions on the particular can.

Utilizing a database of 45 in service steel wind turbine towers the D_c/t up the height of the towers is provided in Fig. 2a. D_c/t is typically at a minimum at the base of the tower. D_c/t increases up the height of the tower despite the fact that the tower tapers (in response to the decreased demands in bending) thus both the D_c and t are decreasing, but t at a faster rate, up the tower height. Near the top of the tower, at the hub connection, the thickness is significantly increased to mitigate against localized actions and fatigue. Histograms of D_c/t at the base and the maximum D_c/t in a given tower are provided in Fig. 2b and c, respectively. Mean base D_c/t is 113 with a CoV of 0.30, and the mean of the max D_c/t per tower is 256 with a CoV of 0.09.

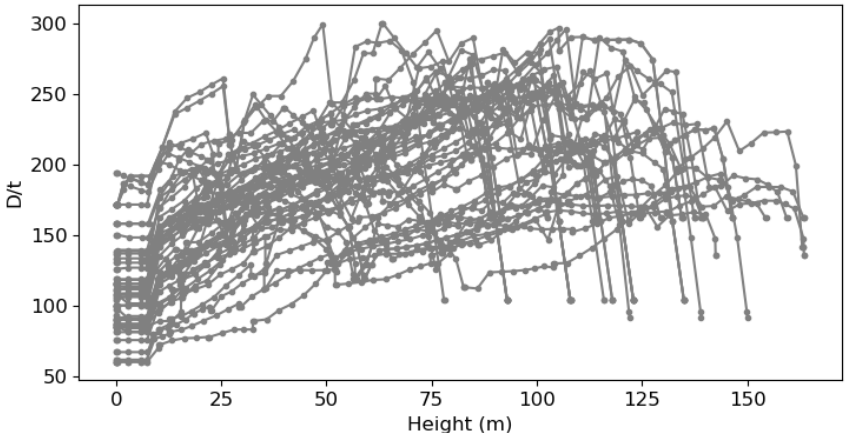

(a) D_c/t variation across height of tower

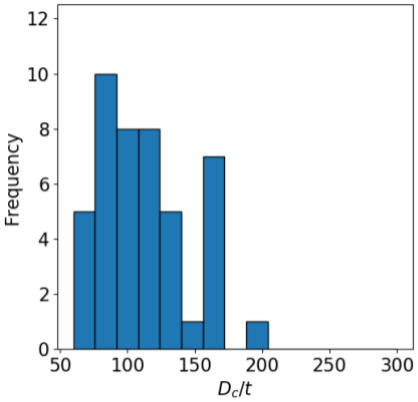

(b) D_c/t histogram at base

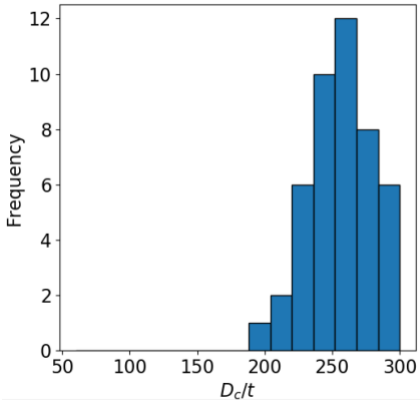

(c) D_c/t histogram for maximum D_c/t

Figure 2: Cross-section slenderness of steel wind turbine towers in current use

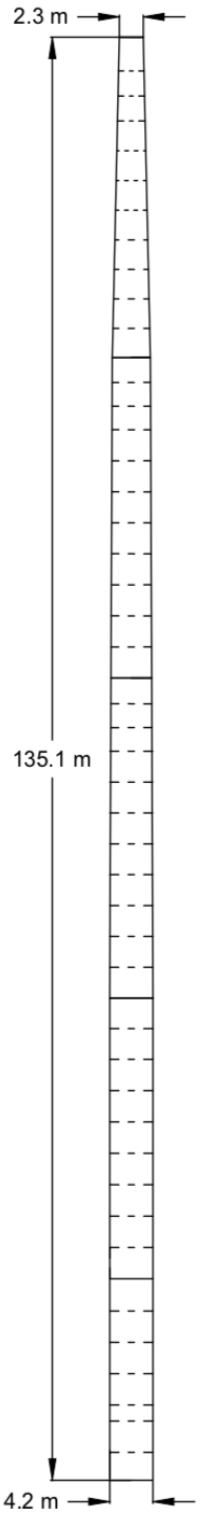

Figure 1: Scaled drawing of typical wind turbine tower

The towers are tall and slender. If L is the length of the towers and we take D_c at the base of the tower the mean L/D_c for the studied towers is 27.6 with a min of 21.5 and max of 33.2. In addition, for a segment between ring stiffeners of length L_s, where 24.6 m is typical, the mean L_s/D_c is 6.1 with a min of 2.3 and max of 9.5. Finally, for a can of length L_c, where 2.63 m is typical, the mean L_c/D_c is 0.70 with a min of 0.23 and max of 1.05.

2.2 Critical Actions

The critical loading actions on a wind turbine tower are summarized in Fig. 3. Moment (M_z) and torsion (T_x) are correlated, thus instantaneous demands on the tower include both of these actions at or near their maxima. Overall the tower experiences axial, torsion, shear, and moment demands as depicted in Fig. 3. The moment demands (M_z) develop from a large concentrated load ($F_{y,concen}$) derived from the wind pressure on the blades and a smaller distributed load ($F_{y,dist}$) due to the wind pressure directly on the tower. The bending at the base is proportional to the tower height L for $F_{y,concen}$ and L^2 for $F_{y,dist}$ resulting in large M_z demands at the base. Torsion arises from eccentricity in the wind loads as the blades sweep around causing twisting at the top of the tower that is not resolved at the moment in time by the nacelle pivoting. Examination of tower designs indicates the relative importance of these two demands: moment dominates at the base, combined torsion and moment control design near the top of the tower. Axial and shear demands have a relatively small influence on the design.

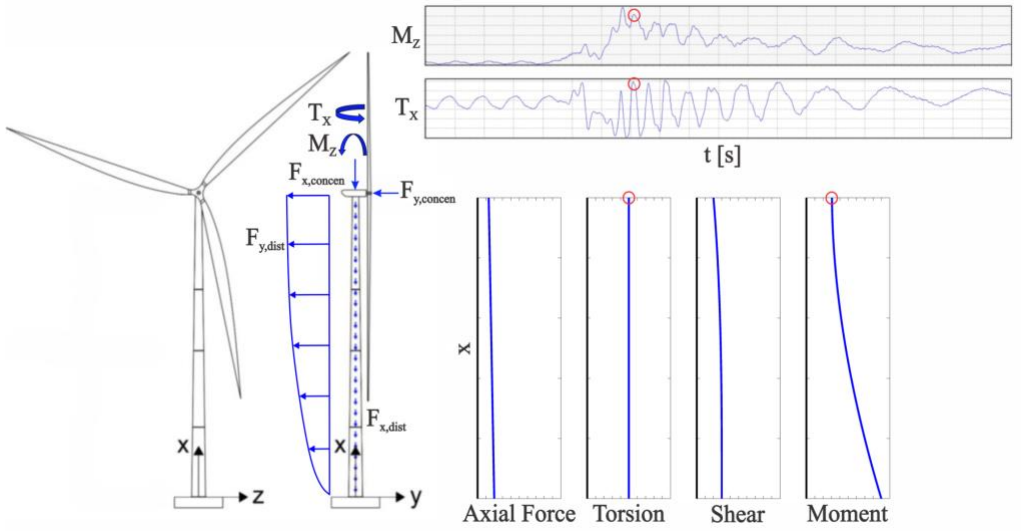

Figure 3: Time histories of the moment M_z and torsion T_x at the tower top during operational conditions with a coherent wind gust and directional change; instantaneous distributions of axial force, torsion, shear, and moment

2.3 Laboratory Scale Geometry

As part of a larger effort the team is working to perform scale experiments (including scanning imperfections and testing under combined loading) on cylindrical tubes consistent with the basic D_c/t of wind turbine towers. To that end we have investigated commercial sources of such tubes and find that welded duct work has similar geometry to current and potential future (more slender) wind turbine towers. Table 1 lists dimensions of commercially available duct work that is planned for use. These same dimensions are considered in the examples provided later in this paper. Fig. 4 provides a photo of a nominally 10 in. diameter tube in our laser scanning rig (Zhao et al. 2015).

Table 1: Summary of laboratory scale tubes with slenderness complementary to steel towers

Nominal size (in.)	L (in.)	D_c (in.)	t (in.)	D_c/t	L/D_c
4	59.25	3.90	0.0312	125	15.2
6	59.25	5.93	0.0312	190	10.0
8	59.06	7.92	0.0312	254	7.5
10	58.75	9.92	0.0312	318	5.9
12	58.75	12.01	0.0312	385	4.9

1. D_c is centerline diameter, 2. 1 in. = 25.4 mm

Figure 4: Laboratory scale tube with slenderness complementary to steel towers

3. Classical Expressions for Elastic Buckling of Cylindrical Shells

Even given the complications of real wind turbine towers the first building block in understanding their structural response is a clear understanding of their elastic buckling behavior. Here we begin with the classical expressions for cylinders. Although D_c/t is only constant for a single can the buckling wavelengths relevant for a thin-walled cylinder are short so the closed-form solutions for constant D_c/t tubes are still a useful starting point. Numerical (shell finite element) elastic buckling solutions are appropriate for considering step changes across the cans, cutouts, stiffeners, and other geometric effects, and are introduced in Section 4.

Although the primary buckling modes of interest here are developed from bending and/or torsion the axial compression case is the fundamental case for understanding the analytical expressions. The axial compression case also has relevance for the bending case if applied appropriately. Reasonable approximations of the buckling stress in compression and torsion can be found in standards such as Eurocode EN 1993 1-6 (ECCS 2007) and discussion of their practical application is provided by Rotter and Schmidt (2013). A compact, but remarkably complete summary of the contributors to the derivations for cylindrical shell elastic buckling is provided in Silvestre (2007). Here we examine some key points in the derivations and examine the form of the final solutions for elastic buckling in compression, bending, and torsion on a cylindrical tube.

The coordinate system employed in the descriptions that follow is consistent with that established in Timoshenko and Gere (1961) as provided in Fig. 5. The deformations are written in terms of the local coordinate system on the cylinder with axial deformation, u, tangential deformation, v, and radial deformation, w, for any point on the cylinder a distance r from the center, a rotation θ from the reference axis, and at a known axial location as illustrated in Fig. 5.

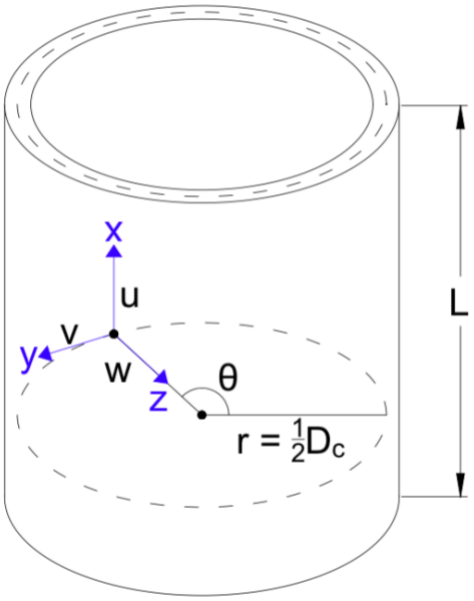

Figure 5: Cylindrical tube, geometry and coordinate system

The fundamental strain-displacement relations for a thin-walled cylinder can be established by considering the membrane strains, bending strains, and nonlinear (higher-order) strains that develop as the shell deforms potentially under axial or shear demands, but here ignoring constant internal/external pressure, these strains include:

$$\epsilon_x = \epsilon_x^m + \epsilon_x^b + \epsilon_x^{NL},\ \epsilon_y = \epsilon_y^m + \epsilon_y^b, \text{ and } \gamma_{xy} = \gamma_{xy}^m + \gamma_{xy}^b + \gamma_{xy}^{NL}. \quad (1)$$

The membrane strains may be expressed as:

$$\epsilon_x^m = \frac{\partial u}{\partial x},\ \epsilon_y^m = \frac{1}{r}\frac{\partial v}{\partial \theta} - \frac{w}{r}, \text{ and } \gamma_{xy}^m = \frac{1}{r}\frac{\partial u}{\partial \theta} + \frac{\partial v}{\partial x} \quad (2)$$

where r is the radius of the cylinder and $D_c = 2r$. The bending strains are:

$$\epsilon_x^b = -z\kappa_x,\ \epsilon_y^b = -z\kappa_y, \text{ and } \gamma_{xy}^b = 2z\kappa_{xy} \quad (3)$$

where the curvatures in the cylinder may be expressed as:

$$\kappa_x = \frac{\partial^2 w}{\partial x^2},\ \kappa_y = \frac{1}{r^2}\left(\frac{\partial v}{\partial \theta} + \frac{\partial^2 w}{\partial \theta^2}\right), \text{ and } \kappa_{xy} = \frac{1}{r}\left(\frac{\partial v}{\partial x} + \frac{\partial^2 w}{\partial x \partial \theta}\right). \quad (4)$$

The additional nonlinear strain terms that develop as the shell deforms, potentially under axial or shear demands, but ignoring constant internal/external pressure include:

$$\epsilon_x^{NL} = \frac{1}{2}\left(\frac{\partial w}{\partial x}\right)^2 + \frac{1}{4}\left(\frac{\partial v}{\partial x} - \frac{1}{r}\frac{\partial w}{\partial \theta}\right) \text{ and } \gamma_{xy}^{NL} = \left(\frac{\partial w}{\partial x}\right)\left(\frac{v}{r} - \frac{1}{r}\frac{\partial w}{\partial \theta}\right) \quad (5)$$

In vector form denoting $\boldsymbol{\sigma} = \lfloor \sigma_x \quad \sigma_y \quad \tau_{xy} \rfloor^T$ and $\boldsymbol{\epsilon} = \lfloor \epsilon_x \quad \epsilon_y \quad \gamma_{xy} \rfloor^T$ equilibrium may be expressed by setting the variation in the total potential energy to zero:

$$\delta\Pi = \iiint \boldsymbol{\sigma}^T \delta\boldsymbol{\epsilon} dV = 0 \quad (6)$$

Separating into our three components and introducing the linear constitutive relation $\boldsymbol{\sigma} = \boldsymbol{C\epsilon}$:

$$\iiint \boldsymbol{\epsilon}^{m^T} \boldsymbol{C} \delta\boldsymbol{\epsilon}^{\boldsymbol{m}} dV + \iiint \boldsymbol{\epsilon}^{b^T} \boldsymbol{C} \delta\boldsymbol{\epsilon}^{\boldsymbol{b}} dV + \iiint \boldsymbol{\sigma}_{\boldsymbol{o}}^T \delta\boldsymbol{\epsilon}^{NL} dV = 0 \quad (7)$$

The first two integrals represent the variational energy due to the elastic membrane and bending effect and lead to elastic stiffness matrices for suitably defined displacement fields. The final integral, written explicitly in term of pre-buckling stresses, $\boldsymbol{\sigma_o}$, represents the additional energy due to buckling. This final term is commonly provided as an additional external work in classical derivations such as Timoshenko and Gere (1961) while its linearized solution leads to the geometric stiffness matrix.

For an admissible displacement field all the derivatives in Eq.'s 2 – 5 may be formed, thus it is possible to provide analytical expressions for all the integrals in Eq. 7 and solve for equilibrium. The buckling problem is found by determining the scaled magnitude of $\boldsymbol{\sigma_o}$ at which the final stress dependent integral erodes the elastic energy (first two integrals in Eq. 7). The key difference in the variety of methods used for elastic buckling comes in the manner in which the displacement fields are approximated.

All the displacement fields u, v, and w are a function of x and θ, and typically the fields are approximated by multiplicative functions, e.g. $w = f_w(\theta)g_w(x)$. The various solution methods take different approaches to addressing $f(\theta)$ and $g(x)$. In the classical solutions trigonometric series are typically used for the entire cylinder – for certain loading and boundary conditions the integrals are tractable and direct analytical solutions are possible. Hybrid solutions such as the Finite Strip Method (Cheung and Tham 1998) or Generalized Beam Theory (Silvestre 2007) often use trigonometric series for $g(x)$ on the whole domain and then piece-wise polynomials developed similar to finite elements for $f(\theta)$. Singly-curved shell finite elements uses piece-wise polynomial functions for both $f(\theta)$ and $g(x)$. Of course finite elements typically handle Eq. 7 first at the element level then employ assembly to the full domain and only after such assembly is the buckling problem addressed, but overall the procedures remain the same.

3.1 Axial Compression (P_{cr})

For a thin-walled cylinder in axial compression with simply supported end boundary conditions the analytical solution is involved, but tractable. One can assume a displacement field for $f(\theta)g(x)$ of the form:

$$u = \sum_m \sum_n A_{mn} sin(n\theta) \cos\left(\frac{m\pi x}{L}\right), \tag{8}$$

$$v = \sum_m \sum_n B_{mn} cos(n\theta) \sin\left(\frac{m\pi x}{L}\right), \text{ and} \tag{9}$$

$$w = \sum_m \sum_n C_{mn} sin(n\theta) \sin\left(\frac{m\pi x}{L}\right) \tag{10}$$

where u, v, and w are defined for any point x, θ in the cylinder; A_{mn}, B_{mn}, and C_{mn} are arbitrary amplitudes, $2n$ is the number of circumferential half-waves, m is the number of longitudinal half-waves, and L is the cylinder length. For this specific loading and boundary condition the integrals in Eq. 7 remain independent and it is possible to evaluate each m and n term separately. As a result Timoshenko and Gere (1961) and others commonly write the displacement field simply as:

$$u = A_{mn} sin(n\theta) \cos\left(\frac{m\pi x}{L}\right),\ v = B_{mn} cos(n\theta) \sin\left(\frac{m\pi x}{L}\right), \text{ and } w = C_{mn} sin(n\theta) \sin\left(\frac{m\pi x}{L}\right) \tag{11}$$

leaving out the summation across terms. Visualization of Eq. (11) is provided in Fig. 6 where the circumferential deformations implied by the integer n in $f(\theta)$ and the longitudinal patterns implied by m in $g(x)$ are both illustrated.

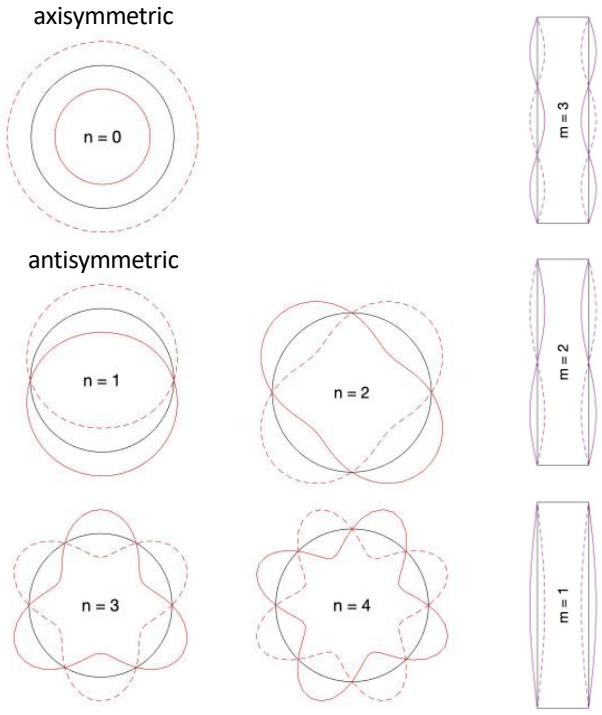

Figure 6: Circumferential (n) and longitudinal (m) wave patterns for axial compression

For the axial compression case the pre-buckling stress is known with $\boldsymbol{\sigma_o} = \lfloor \sigma_{xo} \quad 0 \quad 0 \rfloor^T$ where σ_{xo} is the reference applied stress, often expressed as an end traction $N_x = \sigma_{xo} t$ in the literature.

If one substitutes Eq. 8 into Eq.'s 2-5, and then inserts the result into Eq. 7 along with $\boldsymbol{\sigma_o}$, the resulting equilibrium expression can be used to find the buckling load. Examination of the solution shows that certain classes of buckling deformations can be further separated; specifically, into axisymmetric or antisymmetric buckling. Note, antisymmetric buckling is also known as checkerboard or chessboard buckling in the literature due to the nature of the deformations.

For axisymmetric buckling $v = 0$ and u and w are a function of x only (not a function of θ) and the buckling stress in pure compression is found to be:

$$\sigma_{cr}^{ax} = D\left(\frac{m^2\pi^2}{tL^2} + \frac{E}{r^2D}\,\frac{L^2}{m^2\pi^2}\right) \tag{12}$$

Where D is the rigidity factor (not the diameter D_c) and equal to $Et^3/[12(1-\nu^2)]$ and all other terms are previously defined. The minimum value of the axisymmetric buckling stress occurs at

$$\frac{m\pi}{L} = \sqrt[4]{\frac{Et}{r^2D}} \tag{13}$$

which for ν=0.3 implies a longitudinal half-wavelength of

$$\frac{L}{m} \cong 1.72\sqrt{rt} \tag{14}$$

and a buckling stress of

$$(\sigma_{cr}^{ax})_{\min} = \frac{E}{\sqrt{3(1-\nu^2)}}\frac{t}{r} \tag{15}$$

For the more general case of antisymmetric buckling, the buckling stress may be expressed as:

$$\sigma_{cr}^{as} = \frac{R_1 E}{S_1(1-\nu^2)} \tag{16}$$

Where R_1 and S_1 are defined as:

$$R_1 = (1-\nu^2)\lambda^4 + \alpha[(n^2+\lambda^2)^4 - (2+\nu)(3-\nu)\lambda^4 n^2 + 2\lambda^4(1-\nu^2) - \lambda^2 n^4(7+\nu) + \lambda^2 n^2(3+\nu) + n^4 - 2n^6] \tag{17}$$

$$S_1 = \lambda^2\left\{(n^2+\lambda^2)^2 + \frac{2}{1-\nu}\left(\lambda^2 + \frac{1-\nu}{2}n^2\right)[1+\alpha(n^2+\lambda^2)^2] - \frac{2\nu^2\lambda^2}{1-\nu} + \frac{2\alpha}{1-\nu}\left(\lambda^2 + \frac{1-\nu}{2}n^2\right)[n^2 + (1-\nu)\lambda^2]\right\} \tag{18}$$

and $\alpha = t^2/12r^2$ and $\lambda = m\pi r/L$. For any length, L, one must consider a variety of n and m to determine the minimum σ_{cr}^{as}. Approximations for long and slender tubes exist for the minimum antisymmetric σ_{cr}^{as} (see for example the Eurocode discussion at the end of this section) but here we are primarily interested in the complete solution.

Conversion from the buckling stress (σ_{cr}) to the buckling force (P_{cr}) simply requires multiplying times the cross-sectional area, therefore:

$$P_{cr} = \min(\sigma_{cr}^{ax}, \sigma_{cr}^{as})\, 2\pi rt \tag{19}$$

For the nominally 12 in. diameter steel cylinder of Table 1 ($D_c = 12.01$ in., t = 0.0312 in.) the axisymmetric buckling solution of Eq. 12 is provided as a function of length for $m = 1$ to 1400 in Fig. 7 in gray. The axisymmetric half wavelength equals L/m or Eq. 14. The antisymmetric buckling solution of Eq. 16 is provided as a function of length for n = 1 to 15 and $m = 1$ to 9 in Fig. 7 (top) with various colors. From a classical standpoint the interesting feature is the minimum σ_{cr} response and this is highlighted in the lower portion of Fig. 7 along with the circumferential n and longitudinal m parameters that control any particular portion of the curve. Note, when the tube is long enough, it buckles as a column (n = 1, $m = 1$). Given the prominent role that buckling modes play in understanding imperfection sensitivity an additional and interesting feature that Fig. 7 highlights is the incredibly large number of different deformation modes that have similar buckling stresses for a tube of a given length. This indicates that any of a wide class of imperfections that are sympathetic to one of these modes could be influential in the response.

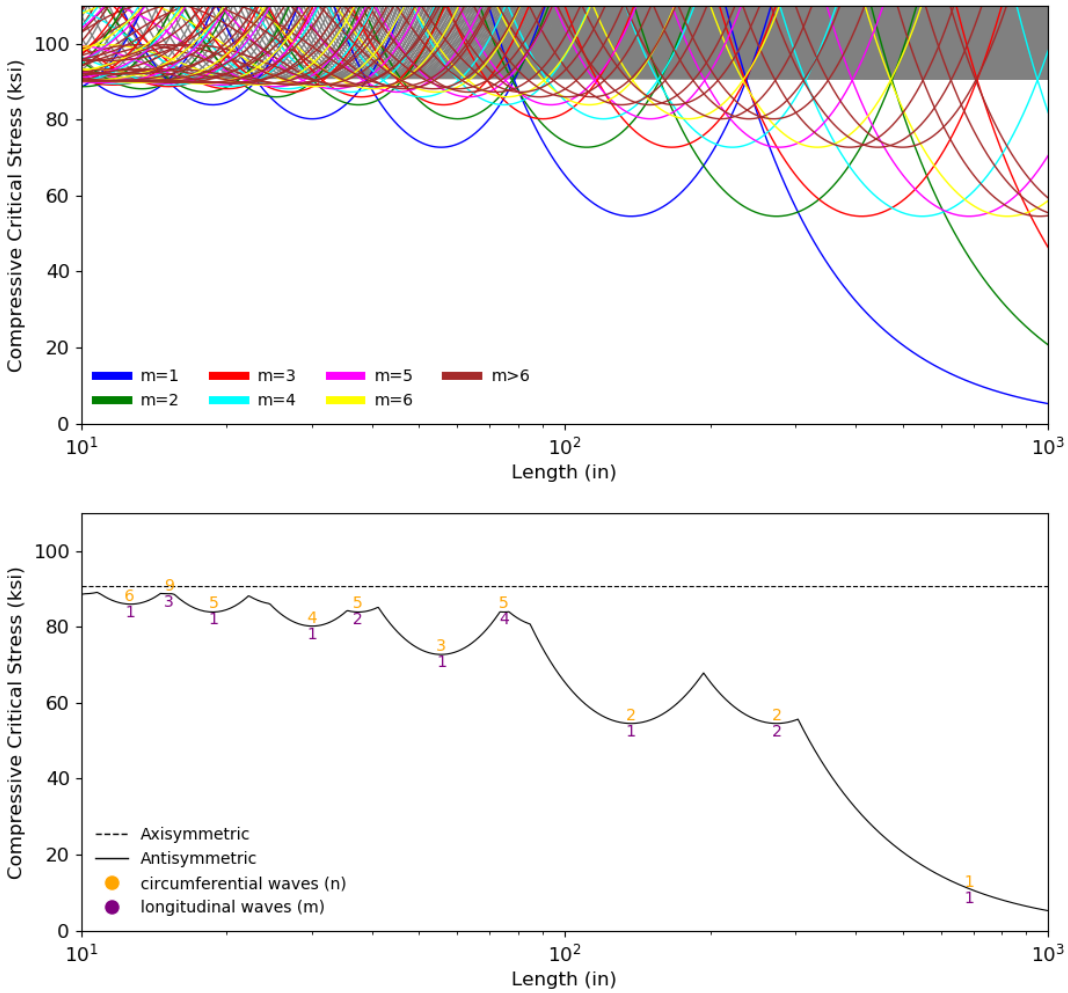

Figure 7: Compressive Stress of a nominal 12 in. diameter tube for multiple wave numbers (top) and envelope of minimum (bottom)

3.2 Bending (M_{cr})

For pure bending of a simply supported cylindrical tube, assuming linear stress variation in the section, the pre-buckling stress $\boldsymbol{\sigma_o} = \lfloor \sigma_{xo} \cos(\theta) \quad 0 \quad 0 \rfloor^T$. The double sine series of Eq.'s 8-10

apply, but here the presence of the cos (θ) term in the pre-buckling stress implies that the final integral in Eq. 7 cannot be treated independently for each m and n term. The solution is possible, but so long as to not be particularly illuminating as a closed-formed expression. As a result, a large number of approximate methods have been developed for this problem.

Flugge (1932/1962) noted in an experiment that the bending critical stress, σ_{cr}^{b}, was 1.3 times the axial critical stress, σ_{cr}^{as}, and recommended using σ_{cr}^{as} as a lower bound. Seide and Weingarten (1961) concluded that $\sigma_{cr}^{b} = \sigma_{cr}^{as}$ was an appropriate expression. Silvestre (2007) employed Generalized Beam Theory to solve the critical bending stress problem for the same geometry as Flugge's tests and showed that the ratio of $\sigma_{cr}^{b}/\sigma_{cr}^{as}$ varies as a function of length, as illustrated in Fig. 8. Further he showed that the ratio of stress is approximately 1.3 for the material and geometry tested by Flugge. Fig. 8 clarifies that the use of σ_{cr}^{as} to approximate σ_{cr}^{b} is not the best approach for anything other than a coarse lowerbound approximation.

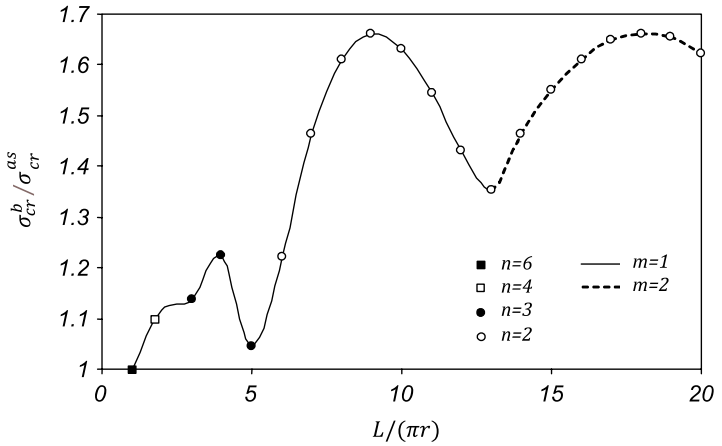

Figure 8: Silvestre (2007) study of the ratio of bending critical stress to axial stress for specimen tested by Flugge (only notation updated here to be consistent with other terms herein)

Surprisingly, an even simpler approximation exists for the critical bending stress. Under bending only a small strip of material is in maximum compression and adjacent to this strip the section is also in compression and provides little resistance. Local to the strip the boundary condition is quite similar to that for axisymmetric local buckling in pure compression and it has been found that:

$$\sigma_{cr}^{b} \cong \sigma_{cr}^{ax} \tag{20}$$

The axisymmetric solution of Eq. 12 is provided as an approximation for σ_{cr}^{b} of the nominally 12 in. diameter steel cylinder of Table 1 ($D_c = 12.01$in, t = 0.0312in) in Fig. 9 for $m = 1$ to 135. Conversion from the buckling stress (σ_{cr}^{b}) to the buckling moment (M_{cr}) requires multiplying times the elastic section modulus, therefore:

$$M_{cr} = \sigma_{cr}^{b} \pi r^2 t \tag{21}$$

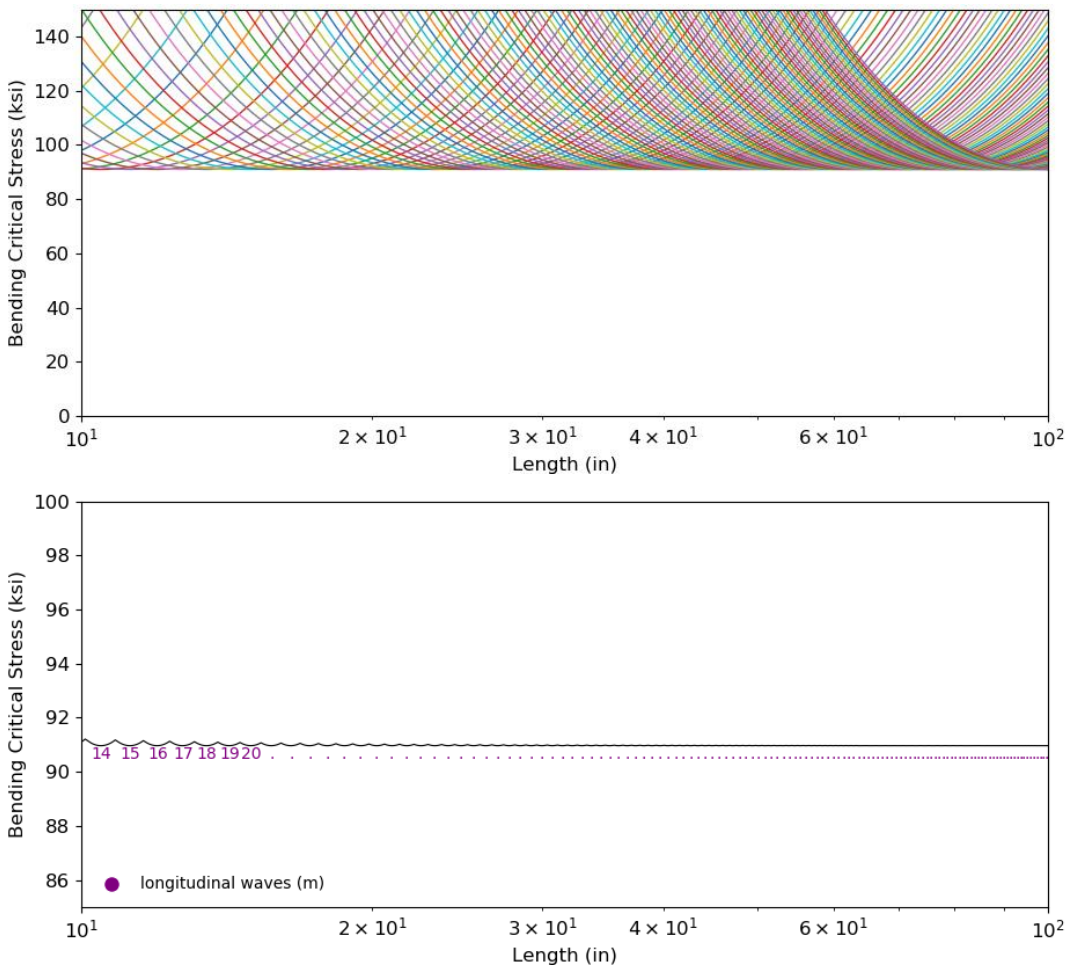

Figure 9. Approximate critical bending stress for multiple wave numbers (top) and envelope of minimum (bottom)

3.3 Torsion (T_{cr})

For torsion the pre-buckling stress is simply that of pure shear, i.e., $\boldsymbol{\sigma_o} = \lfloor 0 \quad 0 \quad \tau_{xyo} \rfloor^T$ thus the ϵ_x^{NL} term drops out in this case and γ_{xy}^{NL} instead plays the critical role in the final term of Eq. (7). The double sine series of Eq. 8-10 remains admissible for the boundary conditions and loading, but requires a large number of terms to provide a reasonable level of accuracy due to the fact that the basic solution is only approximated by $f(\theta)g(x)$. Relying on a physical understanding of the buckling, researchers instead employed trigonometric series that deform in a helix, specifically:

$$u = \sum_m \sum_n A_{mn} \cos\left(\frac{m\pi x}{L} - n\theta\right), \tag{22}$$

$$v = \sum_m \sum_n B_{mn} \cos\left(\frac{m\pi x}{L} - n\theta\right), \text{ and} \tag{23}$$

$$w = \sum_m \sum_n C_{mn} \sin\left(\frac{m\pi x}{L} - n\theta\right) \tag{24}$$

In this form the notion of m longitudinal half-waves and $2n$ circumferential half-waves persists, but the waves are helically wound around the cylinder. These expressions are not valid at the end boundary conditions, and thus apply for a slice of the tube far enough from the end boundary conditions to be unaffected. This form has the added advantage of maintaining the independence

of the m and n terms for the simply supported end boundary condition. Similar to Fig. 6, Fig. 10 provides visualization of the m and n terms along the length x for torsion. Circumferential patterns for torsion are the same as compression. Longitudinal patterns for torsion are different than compression because of the helical deformations.

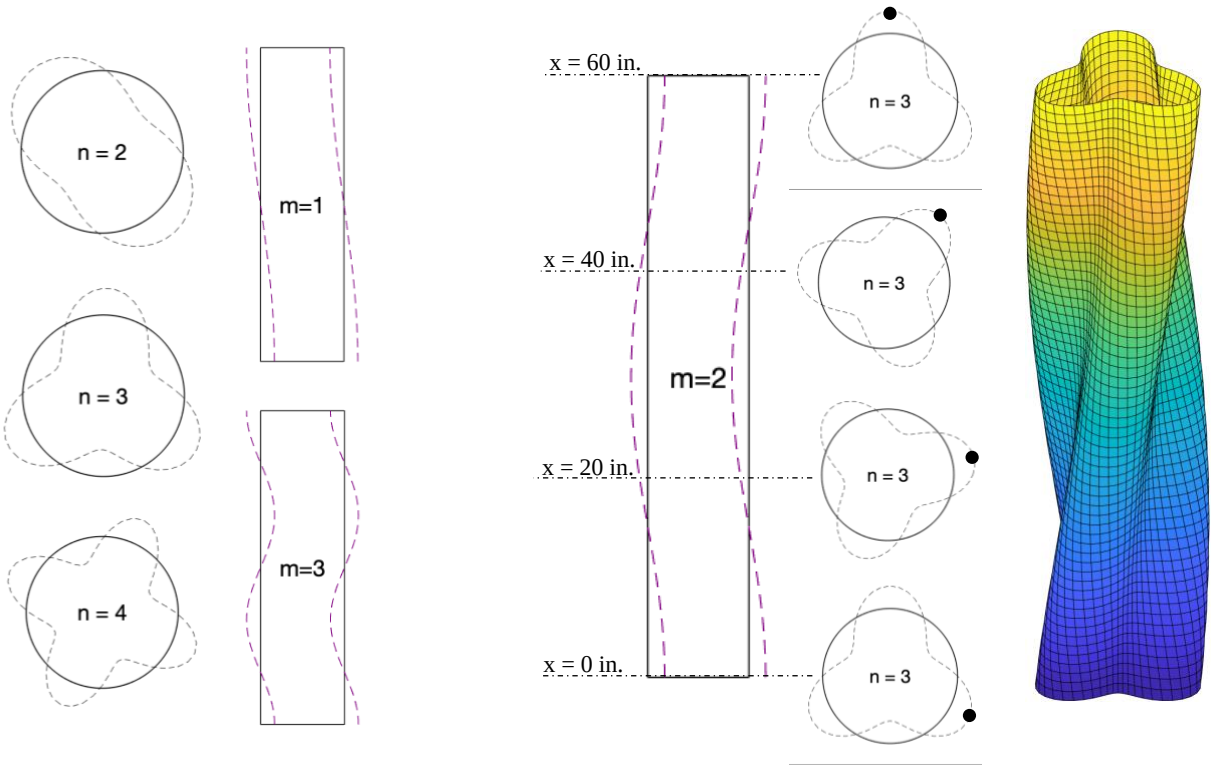

(a) Circumferential and longitudinal waves (b) cross sections and 3D model for n = 3 and m = 2

Figure 10: Circumferential and longitudinal deformations for torsion displacement functions

If one follows the solution of Timoshenko and Gere (1961) several higher order terms are neglected in solving the integrals of Eq. 7 (more precisely higher order terms are neglected in the resulting equilibrium expressions, Timoshenko and Gere do not expressly use the weak form to develop the equilibrium expressions as presented in Eq. 7 for this particular problem). The following elastic buckling solutions is established:

$$\tau_{cr} = \frac{R_2 E}{S_2(1-\nu^2)} \tag{25}$$

where R_2 and S_2 are defined as:

$$R_2 = (1-\nu^2)\lambda^4 + \alpha[(n^2+\lambda^2)^4 - (2+\nu)(3-\nu)\lambda^4 n^2 + 2\lambda^4(1-\nu^2) - \lambda^2 n^4(7+\nu) + \lambda^2 n^2(3+\nu) + n^4 - 2n^6] \tag{26}$$

$$S_2 = 2\lambda n^5 - 2\lambda n^3 + 4\lambda^3 n^3 - 2\lambda^3 n + 2\lambda^5 n \tag{27}$$

For the nominally 12 in. diameter steel cylinder of Table 1 ($D_c = 12.01$ in., t = 0.0312 in.) the torsion buckling solution of Eq. 25 is provided as a function of length for n = 1 to 10 and $m = 1$ to 20 in Fig. 11. The minimum τ_{cr} response is highlighted in the lower portion of Fig. 7 along with

the circumferential n and longitudinal m parameters that control any particular portion of the curve. Similar to Fig. 7, Fig. 11 serves to highlight the large number of different deformation modes that have similar buckling stresses for a tube of a given length and the expected imperfection sensitivity that comes with this observation.

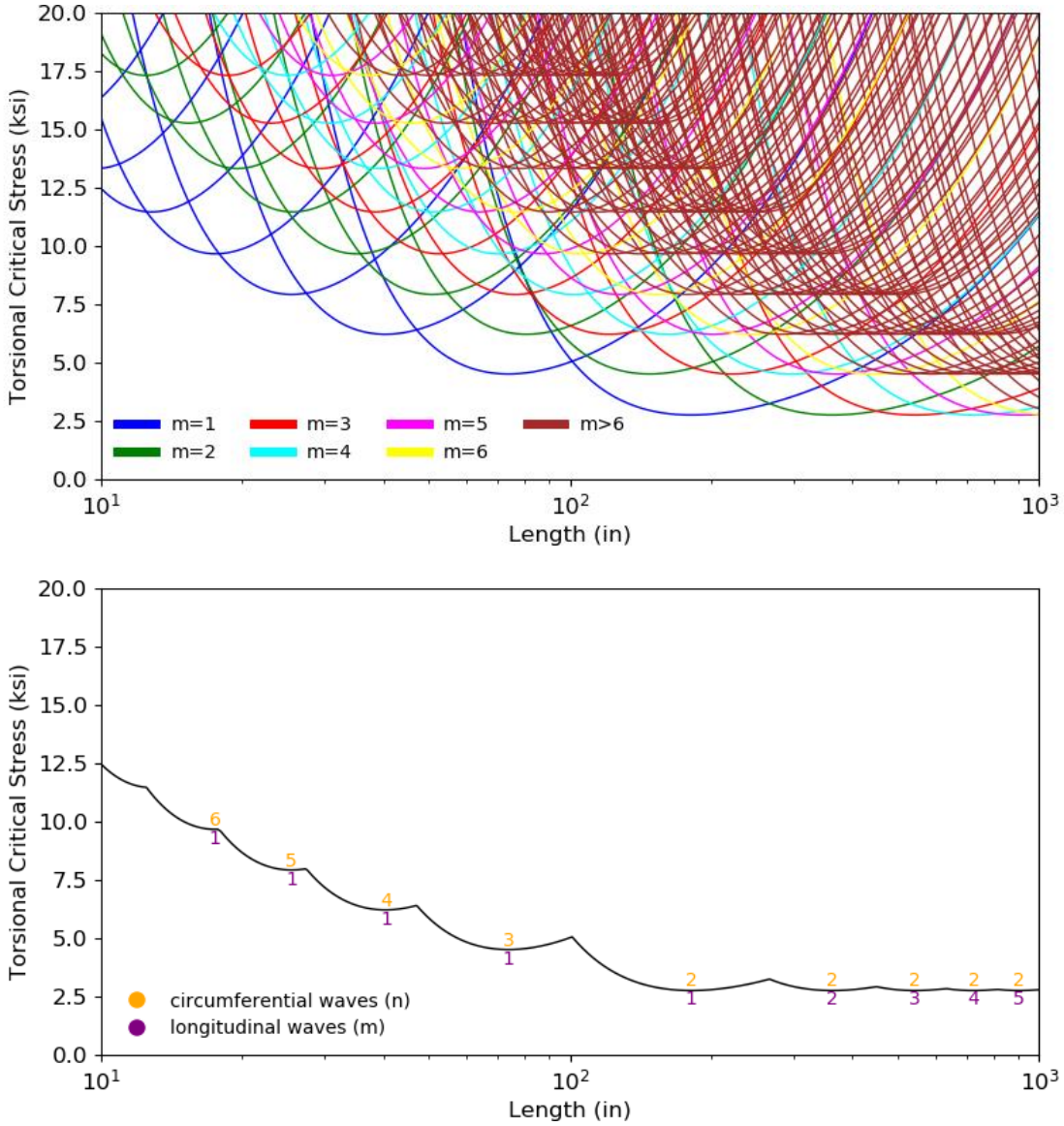

Figure 11: Torsional Stress of a nominal 12 in. diameter tube for multiple wave numbers (top) and envelope of minimum (bottom)

It is worth noting that torsion buckling stresses can be quite low for thin-walled cylinders and thus sensitivity to end boundary conditions which increase the buckling stress are of high interest. The displacement fields of Eq. 22-24 are not admissible for simply supported or fixed ends, and appropriate functions create coupling in the integral terms leading to difficulty in providing exact analytical solutions. However, Donnell (1933) using additional approximations in what higher order strain terms were kept, and did develop approximate expressions that have proven useful:

$$\tau_{cr} = \frac{BEt}{L(1-\nu^2)} \tag{28}$$

where B is provided for simply supported (SS) or fixed ends as:

$$B_{SS} = 0.385nJ_d^{\frac{1}{2}} + \frac{1}{n^2 J_d^{\frac{1}{4}}} + \frac{6.5}{n^5 J_d} \tag{29}$$

$$B_{fix} = 0.385nJ_d^{\frac{1}{2}} + \frac{0.94}{n^2 J_d^{\frac{1}{4}}} + \frac{18.3}{n^5 J_d} \tag{30}$$

and the non-dimensional variable J_d is defined as:

$$J_d = \frac{1}{\sqrt{1-\nu^2}}\left(\frac{L^2 t}{D^3}\right) \tag{31}$$

Donnell's approximate solutions are compared with the minimum solution from Eq. 25 in Fig. 12 using the same geometry as Fig. 11 (D_c = 12.01 in., t = 0.0312 in.). We note that the influence of the fixed end boundary conditions persists up to $L \cong 500$ in (or L/D_c = 41.5). Further, we note that Donnell's solutions are slightly higher, even for the simply supported case, due to the simplifications in his derivation – as has been noted by others (e.g. Silvestre 2007). Conversion from the shear buckling stress (τ_{cr}) to the buckling torque (T_{cr}) is provided by:

$$T_{cr} = \tau_{cr} 2\pi r^2 t \tag{32}$$

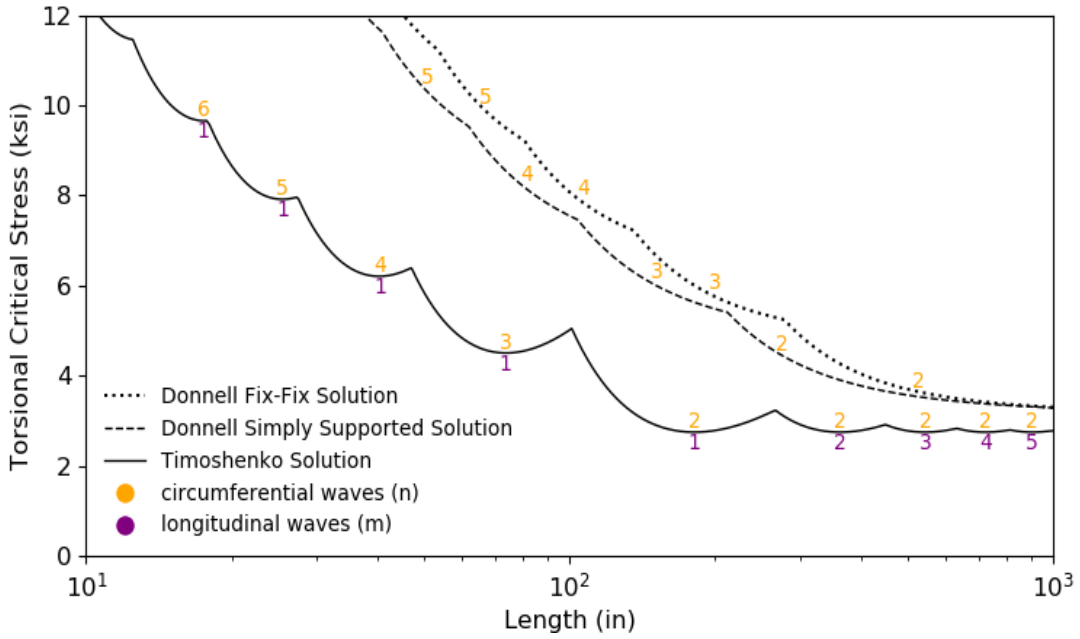

Figure 12: Torsional Stress of a nominal 12 in. diameter tube – envelope of minimum of Donnell's solutions and Timoshenko's solution

3.3 Eurocode shell buckling formulas

For completeness, the simplified buckling formulas for Eurocode 1993 1-6 are also provided in the same notation used in this paper. For axial compression with simply supported boundary conditions, the elastic buckling stress is:

$$\sigma_{cr}^{a} = 0.605EC_x\frac{t}{r} \tag{33}$$

$$\omega \le 1.7 \qquad C_x = 1.36 - \frac{1.83}{\omega} + \frac{2.07}{\omega^2} \tag{34}$$

$$1.7 \le \omega \le 0.5\frac{r}{t} \qquad C_x = 1.0 \tag{35}$$

$$\omega \ge 0.5\frac{r}{t} \qquad C_x = \max\left(1 + 0.2\left(1 - 2\omega\frac{t}{r}\right), 0.6\right) \tag{36}$$

$$\omega = L/\sqrt{rt} \tag{37}$$

For pure torsion, the buckling shear stress is:

$$\tau_{cr} = 0.75EC_\tau\sqrt{\frac{1}{\omega}}\frac{t}{r} \tag{38}$$

$$\omega \le 10 \qquad C_\tau = \sqrt{1 + \frac{42}{\omega^3}} \tag{39}$$

$$10 \le \omega \le 8.7\frac{r}{t} \qquad C_\tau = 1.0 \tag{40}$$

$$\omega \ge 8.7\frac{r}{t} \qquad C_\tau = \frac{1}{3}\sqrt{\omega\frac{t}{r}} \tag{41}$$

Finally for pure bending, Eurocode does not provide a direct formula, but Chen et al. (2008) (the senior author is Rotter who authored much of the Eurocode and related literature) in explaining the use of Eurocode in bending explicitly recommends:

$$\sigma_{cr}^{b} = \frac{E}{\sqrt{3(1-\nu^2)}}\frac{t}{r} = (\sigma_{cr}^{ax})_{\min} \tag{42}$$

Eurocode's expressions are compared with the classical solution for the nominally 12 in. diameter tube example ($D_c = 12.01$ in., t = 0.0312 in.) in Fig. 13. Eurocode's solution for compression (Eq. 33) is equal to the axisymmetric solution for L < 42 in. and for L > 125 in., stress stays constant at 55 ksi. Eurocode's solution for torsion (Eq. 38) closely matches Donnell's solution for torsion with fix-fix boundary conditions.

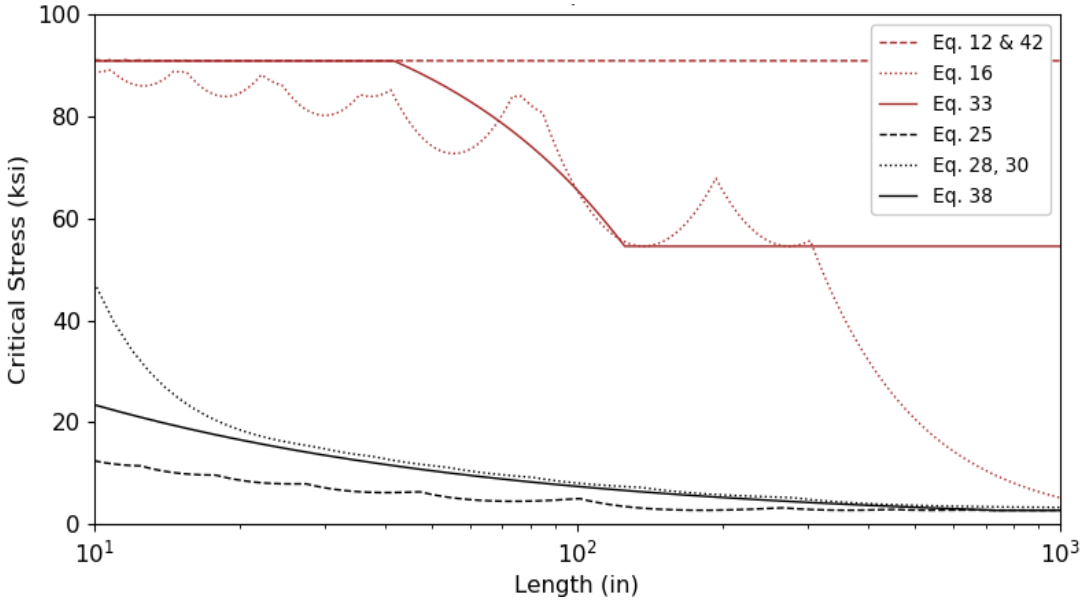

Figure 13: Comparison of Eurocode buckling stresses in compression, bending, and torsion with classical expressions for a $D_c = 12.01$ in., t = 0.0312 in. cylinder.

4. Shell Finite Element Modeling for Elastic Buckling

To provide comparison to the analytical expressions and to begin to exercise a more general purpose tool elastic buckling predictions from shell finite element models are provided in this section. The models are conducted in Abaqus using the linear thin shell finite element S4R. This element along with the quadratic S9R5 element were both found to provide satisfactory performance in the studies of Mahmoud et al. (2017). Mahmoud also concluded that element aspect ratios should be less than 2:1 and element length should be less than $1.0\sqrt{rt}$ – criteria that are maintained in the results provided here. The end boundary conditions are established by coupling the degrees of freedom at each end of the tube to a reference point at the centroid as detailed in Table 2. Distributing coupling between the reference point and the end section is employed for compression and kinematic coupling for bending and torsion.

Table 2: Model end boundary conditions - restrained DOF at centroidal end reference points

Action	End 1 (Reference Point 1)						End 2 (Reference Point 2)					
	d_{X1}	d_{Y1}	d_{Z1}	θ_{x1}	θ_{y1}	θ_{z1}	d_{X2}	d_{Y2}	d_{Z2}	θ_{x2}	θ_{y2}	θ_{z2}
Compression	X	X				X	X	X	X			X
Bending	X	X				X	X	X	X			X
Torsion	X	X		X	X		X	X	X	X	X	X

1. cartesian coordinate system with Z longitudinal, 2. X = fixed degree of freedom

4.1 Compression

For the cylindrical members of Table 1, and considering either constant L/D_c or constant L the elastic buckling stress in compression is provided for a shell finite element model in Abaqus, the analytical expression (Eq. 16), and the Eurocode approximation (Eq. 33) in Table 3. Table 3 demonstrates the shell finite element model, the analytical expression, and the Eurocode approximation all provide reasonable predictions for elastic buckling. (Again here we note that elastic buckling itself is a useful parameter for behavior, but not on its own a direct indicator of strength in any manner). However, it is worth nothing that for a constant L, but increasing D_c, the shell finite element model and the analytical solution show an increase in the buckling stress between the nominally 8 and 10 in. diameter specimens while the Eurocode expression predicts a small decrease (essentially the influence of whether the upward cusps in Fig. 7 are included or ignored in the prediction). In addition to the tabular results, Fig. 14 provides the buckling mode shape for the nominally 12 in. diameter specimen at L = 60 in. This buckling mode has an $n = 3$ and $m = 1$ and is in agreement with the analytical solution.

Table 3: Compression Results Comparison

Nom. size	L (in.)	D_c (in.)	t (in.)	L/D_c	D_c/t	Abaqus			Analytical			Eurocode
						σ_{cr}^{a} (ksi)	n	m	σ_{cr}^{a} (ksi)	n	m	σ_{cr}^{a} (ksi)
4	30	3.90	0.0312	7.7	125	181	2	1	179	2	1	168
6	45	5.93	0.0312	7.6	190	112	2	1	111	2	1	111
8	60	7.92	0.0312	7.6	254	90	2	1	89	2	1	92
10	75	9.92	0.0312	7.6	318	79	2	1	79	2	1	79
12	90	12.01	0.0312	7.5	385	74	2	1	74	2	1	70
4	60	3.90	0.0312	15.4	125	150	1	1	148	1	1	168
6	60	5.93	0.0312	10.1	190	125	2	1	124	2	1	111
8	60	7.92	0.0312	7.6	254	90	2	1	89	2	1	92
10	60	9.92	0.0312	6.0	318	102	4	3	100	4	3	90
12	60	12.01	0.0312	5.0	385	75	3	1	74	3	1	83

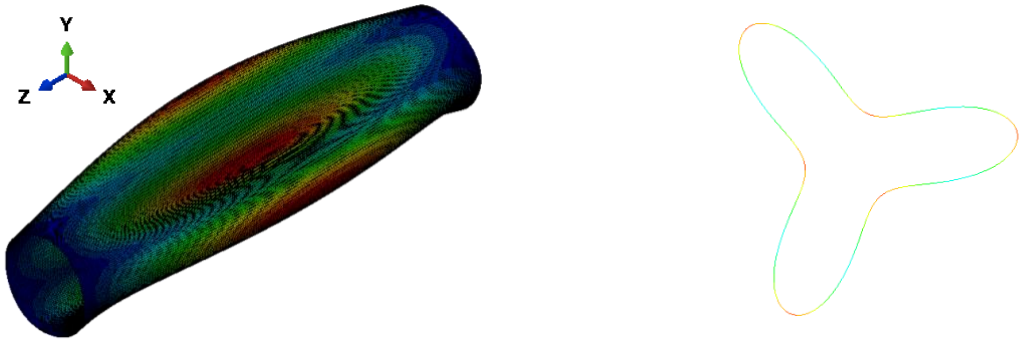

Figure 14: Shell finite element elastic buckling solution in compression: L/D_c = 5.0, D_c/t = 385

4.2 Bending

For the cylindrical members of Table 1, and considering either constant L/D_c or constant L the elastic buckling stress in bending is provided for the Abaqus model and the analytical expression (Eq. 12) in Table 4. The analytical solution for bending and m is approximated using the axisymmetric solution. The shell finite element solutions are all slightly higher than the analytical solutions, with 8% being the largest difference. Interestingly, the number of longitudinal buckling half-waves, m, for the Abaqus solutions are all 80% of the m for the approximate analytical solution. Fig. 15 provides the first buckling mode shape for the nominally 12 in. diameter specimen with L = 60 in. This buckling mode has an m = 64 and n = 1.

Table 4: Bending Results Comparison

nom. size	L (in.)	D_c (in.)	t (in.)	L/D_c	D_c/t	Abaqus			Analytical/Eurocode		
						σ_{cr}^b (ksi)	n[a]	m	σ_{cr}^b (ksi)	n[a]	m
4	30	3.90	0.0312	7.7	125	296	1	56	274	1	70
6	45	5.93	0.0312	7.6	190	193	1	68	182	1	85
8	60	7.92	0.0312	7.6	254	143	1	79	137	1	99
10	75	9.92	0.0312	7.6	318	114	1	89	109	1	110
12	90	12.01	0.0312	7.5	385	94	1	97	90	1	120
4	60	3.90	0.0312	15.4	125	295	1	113	274	1	141
6	60	5.93	0.0312	10.1	190	193	1	92	182	1	115
8	60	7.92	0.0312	7.6	254	143	1	79	137	1	99
10	60	9.92	0.0312	6.0	318	114	1	71	109	1	90
12	60	12.01	0.0312	5.0	385	94	1	64	90	1	80

a. a single transverse half-wave in the compression region is predicted, not the same as n=1 in compression.

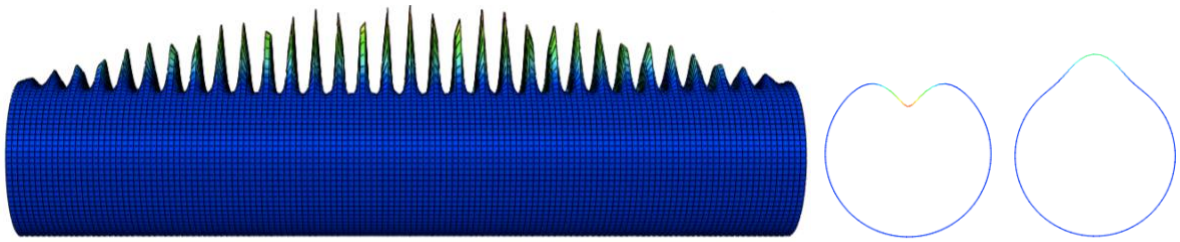

Figure 15: Shell finite element elastic buckling solution in pure bending: L/D_c = 5.0, D_c/t = 385

4.3 Torsion

For the cylindrical members of Table 1, and considering either constant L/D_c or constant L the elastic buckling stress in torsion is provided for the Abaqus model, an analytical expression (Eq. 28), and the Eurocode approximation (Eq. 38) in Table 4. The provided analytical solution is Donnell's fix-fix solution, which only considers n and not m. Timoshenko's solution in Eq. 25 is not used for comparison because it is for an infinitely long cylinder and greatly underestimates critical stress of the cylinders studied here. Table 5 demonstrates the shell finite element model, the analytical expression, and the Eurocode approximation all provide consistent predictions for elastic buckling. In addition to the tabular results, Fig. 16 provides the buckling mode shape for the nominally 12 in. diameter specimen with L = 60 in. This buckling mode has an n=5 and m=2.

Table 5: Torsion Results Comparison

nom. size	L (in.)	D_c (in.)	t (in.)	L/D_c	D_c/t	Abaqus			Analytical			Eurocode
						τ_{cr} (ksi)	n	m	τ_{cr} (ksi)	n	m	τ_{cr} (ksi)
4	30	3.90	0.0312	7.7	125	33.6	3	2	34.3	3	N/A	31.6
6	45	5.93	0.0312	7.6	190	21.0	3	2	20.4	4	N/A	18.8
8	60	7.92	0.0312	7.6	254	14.4	4	3	14.3	4	N/A	13.1
10	75	9.92	0.0312	7.6	318	10.7	4	2	10.8	4	N/A	9.9
12	90	12.01	0.0312	7.5	385	8.5	4	3	8.5	4	N/A	7.8
4	60	3.90	0.0312	15.4	125	23.8	2	2	24.1	2	N/A	22.3
6	60	5.93	0.0312	10.1	190	17.3	3	2	17.7	3	N/A	16.3
8	60	7.92	0.0312	7.6	254	14.4	4	3	14.3	4	N/A	13.1
10	60	9.92	0.0312	6.0	318	12.1	4	3	12.1	4	N/A	11.1
12	60	12.01	0.0312	5.0	385	10.5	5	2	10.5	5	N/A	9.6

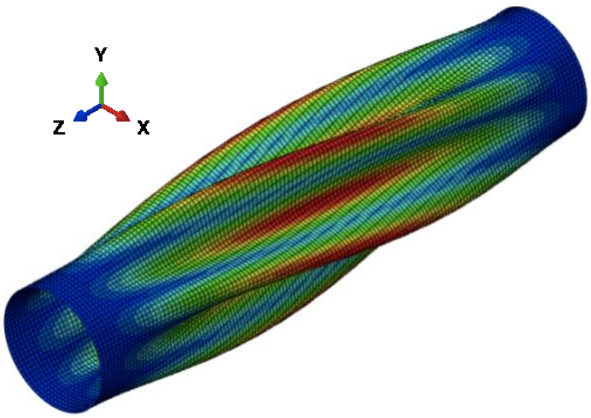

(a) Nominally 12 in. diameter specimen with coordinate system

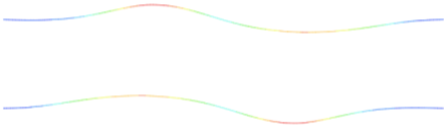

(b) Longitudinal cross section

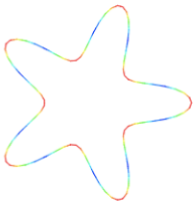

(c) Circumferential cross section

Figure 16: Shell finite element elastic buckling solution in torsion: L/D_c = 5.0, D_c/t = 385

5. Future Work

In the future we aim to study the imperfection sensitivity of cylindrical shells consistent with slender wind turbine tower applications. In this context our interest in the elastic buckling solutions is as much for the mode shapes as for the elastic buckling loads. The elastic buckling modes form an important deformation basis from which one can study imperfection sensitivity. We intend to perform laser scanning, experimental testing, and shell finite element collapse simulations on the tubes of Table 1 to elucidate these sensitivities in the future.

6. Conclusions

The analytical solutions for the elastic buckling of a thin cylindrical shell in compression, bending, and torsion are outlined and provided in common notation. The cross-section signature curve and buckling half-wavelength vs. buckling load, is provided for a thin cylindrical shell. The curve demonstrates that at any given length an incredibly large number of buckling mode shapes that provide similar buckling loads are present. This implies that a relatively wide class of physical geometric imperfections may be sympathetic with buckling modes in the shell that are immediately relevant to the structural response. The analytical elastic buckling solutions are compared with shell finite element models and found to be in good agreement, both in terms of buckling mode and buckling load. The work provides the first step towards imperfection sensitivity studies in slender wind turbine towers. Experiments and collapse simulations are planned in future work.

Acknowledgments

This material is based upon work supported by the National Science Foundation under Grant No. 1912481 and No. 1912354. Any opinions, findings, and conclusions or recommendations expressed in this material are those of the authors and do not necessarily reflect the views of the National Science Foundation.

References

Chen, L., Doerich, C., Rotter, J.M. (2008). "A study of cylindrical shells under global bending in the elastic-plastic range." *Steel Construction.* (1).

Cheung, Y.K., Tham, L.G. (1997). Finite Strip Method. CRC Press.

DNV (2002). "Guidelines for Design of Wind Turbines", 2nd Ed. Det Norske Veritas and Risø National Laboratory.

Donnell, L. H. (1933). "Stability of Thin-Walled Tubes Under Torsion." National Advisory Committee for Aeronautics. Report No. 479,

ECCS (2007). Eurocode 3: Design of steel structures - Part 1-6: Strength and Stability of Shell Structures.

Flugge, W. (1932). "Die Stabilitat der Kreiszylmderschale," Ingenieur- Archiv, vol. 3, 1932, pp. 463-506.

Flugge, W. (1962). Stresses in Shells. Springer-Verlag, 499pp.

Jay, A., Myers, A. T., Torabian, S., Mahmoud, A., Smith, E., Agbayani, N., & Schafer, B. W. (2016). Spirally welded steel wind towers: Buckling experiments, analyses, and research needs. Journal of Constructional Steel Research (125), 218-236.

Koiter, W. T. (1945). The Stability of Elastic Equilibrium. TU-Delt. English Translation by E. Riks, provided by U.S. Air Force Flight Dynamics Laboratory.

Rotter, J. M. (2016). "The new method of reference resistance design for shell structures." Proceedings of the International Colloquium on Stability and Ductility of Steel Structures. (SDSS). Timisoara, Romania.

Rotter, J. M., Schmidt, H. (2013). Buckling of Steel Sheels, European Design Recommendations. ECCS - European Convention for Constructional Steelwork.

Seide, P., Weingarten, V.I. (1961). "On the Buckling of Circular Cylindrical Shells Under Pure Bending." Transactions of the ASME, 112-116.

Silvestre. (2007). Generalised beam theory to analyse the buckling behaviour of circular cylindrical shells and tubes. Thin-Walled Structures, 45, 185-198.

Timoshenko, S.P., Gere, J. M. (1961). Theory of Elastic Stability. McGraw Hill (reprinted by Dover in 2009), 541 pp.

Zhao, X., Tootkaboni, M., Schafer, B.W. (2015). "Development of a Laser-based Geometric Imperfection Measurement Platform with Application to Cold-Formed Steel Construction." *Experimental Mechanics* 55 (9) 1779-1790.